DTU Library

Feasibility study for Al-free 808 nm lasers with asymmetric barriers suppressing waveguide recombination

Zubov, F.; Muretova, M. E.; Asryan, L.; Semenova, E. S.; Maximov, M.; Zhukov, A. E.

[Link back to DTU Orbit](#)

Feasibility study for Al-free 808 nm lasers with asymmetric barriers suppressing waveguide recombination

F. I. Zubov, M. E. Muretova, L. V. Asryan, E. S. Semenova, M. V. Maximov, and A. E. Zhukov

---

Articles you may be interested in

Linear analysis of traveling sheet electron beam in sine waveguide tubes
Journal of Applied Physics **124**, 133301 (2018); 10.1063/1.5025373

Temperature dependent photoluminescence of anatase and rutile TiO_2 single crystals: Polaron and self-trapped exciton formation
Journal of Applied Physics **124**, 133104 (2018); 10.1063/1.5043144

Anomalous pressure effect on the magnetic properties of Ni-Mn based shape memory alloys
Journal of Applied Physics **124**, 133901 (2018); 10.1063/1.5041510

High performance continuous-wave InP-based 2.1 μm superluminescent diode with InGaAsSb quantum well and cavity structure suppression
Applied Physics Letters **113**, 161107 (2018); 10.1063/1.5052056
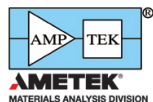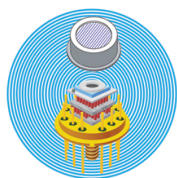
Electroluminescent refrigeration by ultra-efficient GaAs light-emitting diodes
Journal of Applied Physics **123**, 173104 (2018); 10.1063/1.5019764

Reducing the sensitivity of semiconductor ring lasers to external optical injection using selective optical feedback
Journal of Applied Physics **124**, 133101 (2018); 10.1063/1.5046073

Feasibility study for Al-free 808 nm lasers with asymmetric barriers suppressing waveguide recombination

F. I. Zubov,[1,a)] M. E. Muretova,[1] L. V. Asryan,[2] E. S. Semenova,[3] M. V. Maximov,[1] and A. E. Zhukov[1,4]

[1]*Nanophotonics Lab, St. Petersburg National Research Academic University of the Russian Academy of Sciences, St. Petersburg 194021, Russia*
[2]*Virginia Polytechnic Institute and State University, Blacksburg, Virginia 24061, USA*
[3]*Department of Photonics Engineering, Technical University of Denmark, DTU Fotonik, Kgs. Lyngby, DK 2800, Denmark*
[4]*Optoelectronics Department, St. Petersburg State Electrotechnical University "LETI," St. Petersburg 197376, Russia*

The feasibility of implementation of asymmetric barriers (ABs) made of common materials for completely aluminum-free diode lasers is studied. The ABs adjoining a low-dimensional active region on both sides aim to prevent bipolar population in the waveguide layers and thus to suppress parasitic recombination therein, which in turn would enhance the efficiency and temperature-stability of the device. Our search algorithm for appropriate AB materials relies on the minimization of undesired carrier flow (electrons or holes passing through the active region toward the p- or n-type doped cladding layer, respectively), while maintaining the useful flows of hole and electron injection into the active region. Using an example of an 808-nm GaInAsP laser, it is shown that the n- and p-side ABs can be made, for instance, of GaInPSb and GaInP, respectively. In such a laser, the parasitic recombination flux can be suppressed by a factor of 60 for electrons and 200 for holes. It is found that the contribution of the indirect valleys to the electron flow through the p-side AB can be significant and even decisive in some cases. The contribution of light holes to the transmission through the ABs can also be considerable. The optimal thicknesses of the AB layers are determined and the chemical composition tolerances are estimated for a given flux suppression ratio. *Published by AIP Publishing.* https://doi.org/10.1063/1.5039442

I. INTRODUCTION

A steady increase in the optical power has been demonstrated in modern semiconductor laser devices consisting of single emitters, emitter bars, and stacks. Recently, a cryogenically cooled 1 mm wide laser bar with nearly 2 kW peak power has been reported.[1] However, solid-state laser pumping, materials processing, and other power demanding applications require still further enhancement of both the output optical power and the conversion efficiency. The best results obtained so far are for GaInAs quantum well (QW) lasers on GaAs substrates emitting in the 0.9xx μm spectral range. For example, a record-high conversion efficiency of 85% was achieved in a 975 nm diode laser by cooling it down to $-50°$ C.[2] However, the realization of high-performance shorter-wavelength lasers (808 nm and shorter) is a more challenging task.[3]

One of the key fundamental factors limiting the efficiency of semiconductor lasers is the pile-up of charge carriers in their waveguiding layers.[4] For instance, it was shown in Ref. 5 that a significant electron concentration ($>10^{18}$ cm^{-3}) builds up in the p-side waveguiding layer of large optical cavity lasers that operate at high injection currents. Besides the decrease in the conversion efficiency and the saturation of the light-current characteristic caused by additional absorption loss and carrier

recombination, the pile-up of carriers in the waveguiding layers leads to the deterioration of the temperature-stability of the device as the parasitic recombination current increases exponentially with the temperature in contrast to the radiative recombination current in the QW, which increases linearly.[6]

Recently, to suppress the bipolar population in the laser waveguide, we have employed the asymmetric barrier (AB) layers.[7,8] The concept behind the AB lasers is in the utilization of auxiliary layers on both sides of the active region (Fig. 1). These layers provide an obstacle (energy barrier) for the propagation of one type of carriers (e.g., electrons) while not affecting the injection of carriers of the other type (holes). The AB located on the n-side is intended to stop holes, and the p-side AB blocks electrons. As a result, only the useful radiative recombination in the active region should occur. So far, the lasers with both n- and p-side ABs have only been fabricated for the AlGaAs material system (830–850 nm spectral range).[7,8] These devices (based on a GaAs QW in the Al$_{0.2}$Ga$_{0.8}$As waveguide) incorporated a 5–7 nm-thick n-side GaInP AB forming a 240 meV barrier for holes and a 5–7 nm-thick p-side AlGaInAs AB forming an 80 meV barrier for electrons. The use of two ABs allowed for a considerable increase in the characteristic temperature of the threshold current: T_0 was 99 K in the reference structure not containing ABs and it was 143 K in the structure with the ABs. The linearity of the light-current characteristic at high injection level was also improved, which led to a

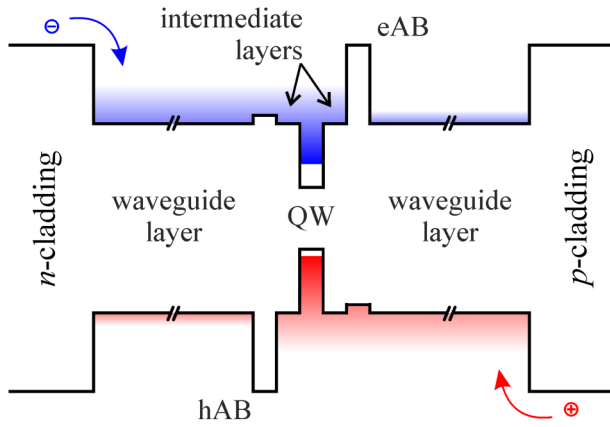a)Author to whom correspondence should be addressed: fedyazu@mail.ru

FIG. 1. Schematic energy band diagram illustrating the concept of a laser with ABs; p- (n-) side AB [marked as eAB (hAB)] aims to suppress the parasitic transport of electrons (holes).

significant (up to 60%) reduction in the current required to achieve a given output power. No effect of ABs on the catastrophic optical mirror damage (COMD) was observed.

Aluminum-free GaInAsP/GaAs heterostructures[9] emerged in the beginning of the 1990s as a promising substitute for AlGaAs/GaAs heterostructures that were commonly used at that time for near-infrared lasers. The use of GaInAsP-based material systems was primarily motivated by the following drawbacks inherent in Al-containing lasers as compared to Al-free ones: increased surface-recombination velocity[10] and electrical resistance,[11] reduced threshold of COMD,[12] as well as reduced resistance to oxidation[13] and dark-line defect formation.[14] Although the quality of facet mirror passivation was greatly improved and AlGaAs-based diode lasers later proved their reliability, Al-free laser heterostructures still remain an alternative solution for high-power diode lasers (see, e.g., Refs. 13, 15, and 16).

In the present work, we study the feasibility of implementation of the AB laser concept for Al-free heterostructures. The article is organized as follows. In Sec. II, we briefly discuss a reference 808-nm Al-free laser structure for which the ABs will be considered. Section III describes our method for the search of ABs, which is based on the minimization of the unwanted carriers flow while impacting insignificantly the useful flux. In Sec. IV, the results of our AB search for 808 nm Al-free laser heterostructures are presented and discussed. Section V summarizes our work.

II. REFERENCE LASER STRUCTURE

Here, we investigate the feasibility of implementation of the AB-concept for completely Al-free structures using an 808 nm separate confinement heterostructure (SCH) laser as an example. The 808 nm heterostructure is of particular interest in view of weak localization of carriers in its active region. We consider as a waveguide material a GaInAsP quaternary alloy lattice-matched to the GaAs substrate and having the bandgap of 1.75 eV.[17] This corresponds to the chemical composition of $Ga_{0.73}In_{0.27}As_{0.46}P_{0.54}$ [that can alternatively be presented as $(GaAs)_{0.46}(Ga_{0.51}In_{0.49}P)_{0.54}$]. The QW active region can also be made of GaInAsP with a higher As content. A $Ga_{0.51}In_{0.49}P$ ternary alloy, the widest

bandgap material ($E_g = 1.92$ eV) that does not contain aluminum and is lattice-matched to GaAs, can be used for cladding layers in the 808 nm laser design.

Figure 2 shows the contour plot representing the lattice mismatch δ for the QW materials ($Ga_xIn_{1-x}As_yP_{1-y}$), which (when used in combination with the above chosen waveguide layers) allow achieving the QW ground-state optical transition at $\lambda_0 = 808 \pm 2$ nm. The data correspond to QWs of a moderate width w ranging from 5 to 8 nm, which can be stacked to increase the optical gain. It is seen from the figure that the mismatch δ lies within the range from -1 to 0.25%. Thus, the QW can be either compressively ($\delta < 0$) or tensile ($\delta > 0$) strained, which, if necessary, can be used to compensate for the strains induced by the AB layers. The compressive strain of about -1% or higher is typically used in high-performance longer-wavelength InGaAs/AlGaAs/GaAs QW lasers. However, achievement of -1% strain with a GaInPAs QW for 808 nm emission is quite challenging because the semiconductor material tends to segregate into InAs- and GaP-rich clusters.[3] In the calculations below, we considered the 7.3 nm-thick $(GaAs)_{0.9}(Ga_{0.51}In_{0.49}P)_{0.1}$ QW layer (marked by a cross in Fig. 2) exactly lattice-matched to the substrate. This QW is characterized by the localization energies (E_{loc}) of 90 and 124 meV for electrons and holes, respectively.

In Ref. 4, the following criterion for suppression of carrier leakage from the active region was determined experimentally: $E_{loc}/(k_BT) > 7$, where k_BT is the thermal energy. Thus, to prevent carrier escape, the localization energy should be 175 meV or higher. We should emphasize that the above criterion can hardly be satisfied in any completely Al-free 808 nm laser as it requires the waveguide bandgap of 1.89 eV or higher. Thus, a significant carrier leakage into the waveguide occurs in our reference 808 nm SCH laser.

III. METHOD FOR SEARCH AND CALCULATION OF AB PARAMETERS

The main purpose of using ABs is minimization of the parasitic fluxes. However, we do not simply maximize here
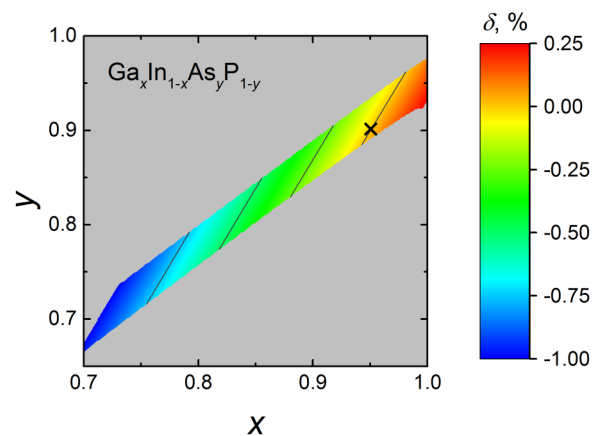
FIG. 2. Contour plot for the lattice mismatch δ of the QW materials ($Ga_xIn_{1-x}As_yP_{1-y}$) that can be used to achieve the ground-state optical transition at 808 nm for the case of GaInAsP barrier layers having 1.75 eV bandgap; $\delta < 0$ and > 0 correspond to compressively- and tensile-strained QW layers, respectively. The cross represents the QW composition $(GaAs)_{0.9}(Ga_{0.51}In_{0.49}P)_{0.1}$ chosen for calculations below.
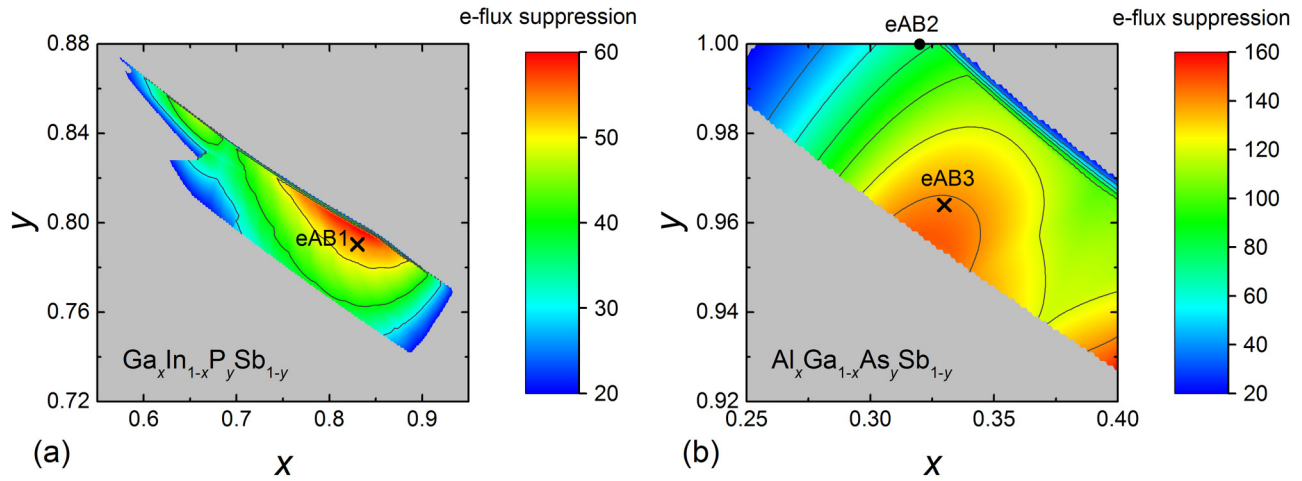
FIG. 3. Contour plots for the parasitic electron flux suppression ratio for ABs based on $Ga_xIn_{1-x}P_ySb_{1-y}$ (a) and $Al_xGa_{1-x}As_ySb_{1-y}$ (b).

the corresponding barrier heights: we use the ratios of suppression of the parasitic fluxes as a measure of the AB performance. This ratio for each type of carriers is defined as the ratio of the parasitic flux in the reference structure to that in the structure with the ABs. For a certain type of ternary or quaternary alloy, the flux suppression ratios (denoted by C_e and C_h for electrons and holes, correspondingly) are calculated for various combinations of chemical compositions and layer thicknesses. The optimal AB thickness, which maximizes the suppression ratio for a given composition, is then chosen (this is discussed below in more detail, see Fig. 4). Note that a composition providing a higher energy barrier that has a smaller critical thickness at the same time can be characterized by a lower parasitic flux suppression ratio as compared to more lattice-matched compositions providing lower barrier heights that have greater critical thicknesses.

We used the following search limitations criteria. (i) The lattice mismatch of the AB material with respect to the GaAs substrate should not exceed 2% to avoid the risk of surface corrugation and, in the extreme case, formation of quantum dots. (ii) The suppression ratio of the useful flux (i.e., C_e for

the n-side AB and C_h for the p-side AB) in the presence of the AB layer should not exceed 25%. (iii) The minimal AB thickness was limited to 3 nm; the maximal thickness was limited to the lesser of the critical thickness and 15 nm in order to make ABs thin enough to avoid inelastic strain relaxation and the possible negative impact of ABs on the optical modes, electrical resistivity, and thermal conductivity of the structure. (iv) Finally, the AB layer should not form a deep potential well for carriers entering the QW active region as this could complicate designing the QW. In this work, the depth of the "spurious" well was limited to 50 meV. Figure 1 illustrates a possible situation when a shallow spurious well for holes is provided by type II heterojunctions formed at the interfaces between the p-side AB layer and the waveguide. Note that insertion of intermediate layers between the AB and the QW is undesirable as these layers would act as intermediate energy steps helping carriers to overcome even high potential barriers.

We searched for feasible AB materials among all ternary and quaternary alloys formed by group III (Ga, In, and Al) and group V (As, P, and Sb) elements. Although the aluminum-free laser design is of primary interest in this work, materials with a limited content of Al (not more than 40%) were also examined for the sake of completeness. In the present work, the majority of material parameters of semiconductor alloys, including the band edge positions in the absence of strain, effective masses, deformation potentials for the Γ-point, as well as elastic constants, were determined by interpolation of the data for binary and ternary constituents collected in Ref. 18. The interpolation included the quadratic dependence of the parameters on the compound composition (so-called bowing). The effective masses (both longitudinal and transverse) for the X and L valleys for InP were taken from Ref. 19 and the longitudinal effective masses for the X and L valleys for InSb—from Ref. 20, as these parameters are missing in Ref. 18. Due to the lack of data, we used the following guess values: 1.5 (0.15) for the longitudinal (transverse) effective electron masses in AlP for the L valley and 0.2 (0.15) for the transverse effective electron masses in InSb for the X (L) valley, respectively. These guess values are close to the average values of the
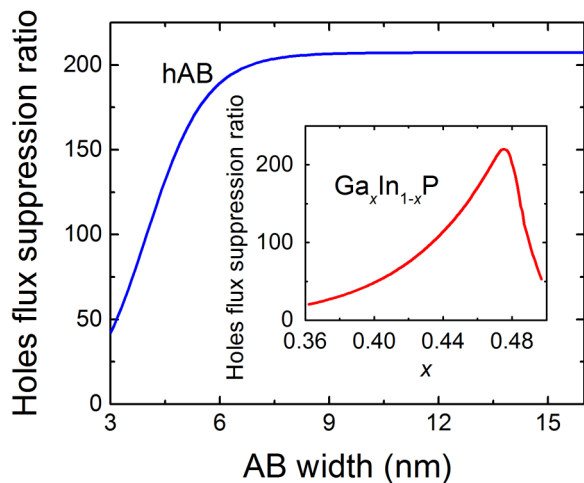

FIG. 4. Hole flux suppression ratio for the n-side AB (hAB) versus its width. Inset: hole flux suppression ratio versus the composition of $Ga_xIn_{1-x}P$ hAB.

corresponding effective masses determined using the known data for binary compounds.

The effect of strain on the semiconductor band structure was taken into account in accordance with the conventional model described in Ref. 21. We considered a (001)-oriented substrate; hence the ABs are strained along the growth direction [001], i.e., the drift direction of charge carriers. The deformation potentials for the X and L valleys were taken from Ref. 19. For a limited number of missing potentials, we used guess values taken to be equal to the average values of corresponding potentials determined from the known data for binary compounds. We varied the guess values (effective masses and deformation potentials for indirect valleys) within reasonable limits and found that our calculation results were affected only insignificantly. The critical thicknesses of the dislocations formation in the strained layers were determined using the Matthews and Blakeslee model[22] with the Burgers vector $b = a/\sqrt{2}$, where a is the lattice constant. The size quantization levels in the active region in the presence of the AB layers were calculated using the transfer matrix method.

The flux density for carriers (electrons or holes) tunneling through the AB layers was calculated using the Tsu-Esaki formula,[23]

$$f = \frac{1}{2\pi\hbar} \int_0^\infty n_w^{2D} D dE, \qquad (1)$$

where

$$n_w^{2D} = \frac{m_w k_B T}{\pi\hbar^2} \ln\left[1 + \exp\left(\frac{E_F - E_0 - E}{k_B T}\right)\right]$$

is the two-dimensional concentration of carriers in the waveguiding layer having the kinetic energy E of motion in the growth direction, E_0 and E_F are the band edge and the quasi-Fermi level, respectively, m_w is the carrier effective mass in the waveguiding layer, k_B is the Boltzmann constant, T is the temperature, and D is the probability of transmission (tunneling) through the potential barrier. In our calculations, room-temperature ($T = 300$ K) operation was considered. The quasi-Fermi levels were assumed to coincide with the corresponding ground-state levels of the active region.

For a potential barrier of rectangular shape with the height U and the width w, the transmission probability for carriers having $E \leq U$ is

$$D = \frac{1}{1 + \frac{1}{4}\left(\eta + \frac{1}{\eta}\right)^2 \sinh^2 \gamma w} \qquad (2)$$

and for $E \geq U$, it is

$$D = \frac{1}{1 + \frac{1}{4}\left(\eta - \frac{1}{\eta}\right)^2 \sin^2 \gamma w}. \qquad (3)$$

Here, $\eta = (m_w \gamma)/(m_b k)$, $\gamma = \sqrt{2m_b|U - E|/\hbar^2}$, $k = \sqrt{2m_w E/\hbar^2}$, and m_b is the carrier effective mass in the barrier (AB layer). The expressions (2) and (3) for the

transmission probabilities were derived using the Bastard boundary conditions (carrier flow conservation at the heteroboundaries).[24]

In calculations of the electron flux through the ABs, we considered the contributions of the X and L minima in addition to the Γ minimum. Although the X and L valleys are 6- and 8-fold degenerated, their contributions to the electron flux were reduced by half, since these valleys are shared between the neighboring cells in the reciprocal space in zincblende-type materials. In our calculations, we used the longitudinal effective mass $m_l^*(X)$ for the X valley, whose wave-vector is along the growth direction, and the transverse mass $m_t^*(X)$ for the others. For all L valleys, the effective mass of electrons in the growth direction (normal direction to the ABs) is determined by the following combination of the longitudinal $m_l^*(L)$ and transverse $m_t^*(L)$ effective masses in the L valleys:

$$m_{[001]}^*(L) = \left(\frac{1}{3m_l^*(L)} + \frac{2}{3m_t^*(L)}\right)^{-1}. \qquad (4)$$

The hole flux through the ABs includes the contributions of heavy and light holes, as well as holes from the spin-split subband. Note that in our previous works on AB-lasers design[7,8] the Γ valley electrons and the heavy holes were only considered.

IV. RESULTS AND DISCUSSION

Figure 3 shows the contour plots for the parasitic electron flux suppression ratio C_e as a function of the composition of the p-side AB based on $Ga_xIn_{1-x}P_ySb_{1-y}$ [Fig. 3(a)] and $Al_xGa_{1-x}As_ySb_{1-y}$ [Fig. 3(b)]. The data are presented for the optimal thicknesses of ABs. Sufficiently high suppression ratios ($C_e \geq 20$) are only shown in the figure. These two quaternary alloys for the p-side AB satisfy all the criteria discussed in Sec. III. The maximum suppression is achieved at the boundary of the region of feasible compositions and amounts to 60 and 158 in the case of GaInPSb and AlGaAsSb, respectively. The regions of feasible compounds occupy small areas in the composition planes, namely, 1.2% and 0.6% in the case of Al-free and Al-containing compounds, correspondingly.

Table I summarizes the characteristics of the alloys, which we consider here as the most feasible compounds for the ABs. For the p-side ABs, we identify $Ga_{0.83}In_{0.17}P_{0.79}Sb_{0.21}$, $Al_{0.32}Ga_{0.68}As$, and $Al_{0.33}Ga_{0.67}As_{0.964}Sb_{0.036}$ alloys (labeled as eAB1, eAB2, and eAB3, respectively). They are marked by the corresponding labels in Fig. 3. As seen from the figure, eAB1 and eAB3 are close to the points, at which C_e reaches its peak values for GaInPSb and AlGaAsSb quaternary alloys, correspondingly. As a special case of AlGaAsSb quaternaries, we distinguish the antimony-free ternary alloy eAB2. Note that the compositions of eAB1 and eAB3 are intentionally made slightly different from those that maximize C_e; in Figs. 3(a) and 3(b), eAB1 and eAB3 are slightly shifted from the exact locations of the points of maxima of C_e. This is done to step aside from the boundaries of the regions of feasible compositions. We found that at the deviation of $\pm1\%$ from the target composition (such accuracy can be easily met by

TABLE I. Feasible materials for ABs and their characteristics.

Composition	$Ga_{0.83}In_{0.17}P_{0.79}Sb_{0.21}$	$Al_{0.32}Ga_{0.68}As$	$Al_{0.33}Ga_{0.67}As_{0.964}Sb_{0.036}$	$Ga_{0.47}In_{0.53}P$
Designation	eAB1	eAB2	eAB3	hAB
Purpose	Suppression of e-flux (p-side AB)			Suppression of h-flux (n-side AB)
e-flux suppression ratio, C_e	53	76	142	23%
h-flux suppression ratio, C_h	2%	8%	13%	207
Mismatch (%)[a]	−0.05	−0.05	−0.33	−0.34
Critical thickness (nm)	∞	∞	41.0	39.0
Optimal thickness (nm)	12.6	12.1	14.3	10.5
Lowest conduction-band valley	X_t	Γ	Γ	Γ
Highest valence-subband	hh	hh	hh	hh
Conduction-band edge discontinuity (meV)	78	116	157	8
Valence-band edge discontinuity (meV)[b]	−4	2	−35	120

[a]Negative value: compression of the AB layer.
[b]Negative value: a potential well for holes.

modern epitaxial technologies), the material still remains within the suitable compounds range; C_e decreases by less than 15% from its maximal value.

We found only one semiconductor alloy, namely, $Ga_xIn_{1-x}P$, that can be used as the n-side AB to prevent undesirable flow of holes toward the n-type doped cladding layer. For the Ga fraction x ranging from 0.36 to 0.5, this ternary alloy satisfies all the search criteria discussed above. The inset in Fig. 4 shows the dependence of the h-flux suppression ratio C_h on the composition of $Ga_xIn_{1-x}P$. The optimal composition, labeled here as hAB, is $Ga_{0.47}In_{0.53}P$ having the hole flux attenuation ratio of 207. Similarly to the n-side AB composition deviation, the deviation of the ternary alloy composition of the p-side AB within ±1% around $x = 0.47$ does not move the AB material off the suitable compounds range; C_h still remains high enough (≥ 170).

As seen from Table I, all the proposed AB-compounds are either lattice-matched or slightly lattice-mismatched to the substrate. As a result, they can be grown in a pseudomorphic mode up to large thicknesses. However, we found that there is no need to grow thick AB layers since the flux suppression ratio rapidly saturates as the layer thickness increases. As an example, we present in Fig. 4 the dependence of C_h on the thickness of hAB layer. The thickness of the AB, at which the suppression ratio reaches 99.9% of its maximal value for a given barrier, is considered here as an optimal thickness. For hAB, the optimal thickness is 10.5 nm, and for the electronic ABs, it is a bit larger, ranging from 12.6 to 14.3 nm. It is seen from Table I that the optimal thicknesses for the AB materials, which we identified using our search criteria, are well below the critical thicknesses of dislocation formation (for eAB1 and eAB2, the critical thickness tends to infinity). It should be noted that, in the presence of such thin ABs, the characteristics of the laser structure (such as the refractive index profile and thermal conductivity) will only be slightly perturbed as compared to those of the reference structure.

Let us discuss the main features of all four AB designs we propose here. One of three suggested compositions for the p-side AB is aluminum-free (labeled as eAB1). It is characterized by a fairly high electron flux suppression ratio

($C_e = 53$). For comparison, the barrier for electrons formed by an AlGaInAs alloy in our previously demonstrated[7] 830 nm AB-laser with $Al_{0.2}Ga_{0.8}As$ waveguide provided the e-flux attenuation of 9. While C_e obtained with the use of eAB1 is quite high, the discontinuity in the valence-band edge is nearly zero, i.e., eAB1 does not practically affect the hole flux—this flux is suppressed by 2% only. The alloy is lattice-matched to the GaAs substrate and an unintentional variation of ±1% in its composition (Ga/In or P/Sb) would introduce a mismatch not exceeding 0.24%. The drawback of this AB is the presence of antimony in the compound since the epitaxial growth of Sb-containing laser heterostructures is less common.

Unfortunately, the elimination of Sb from the AB composition does not allow to achieve any sufficient attenuation of the electron flux in the fully Al-free (i.e., GaInAsP) AB design. An alternative solution is adding a moderate amount of Al into the alloy—this is realized in eAB2 and eAB3 (32% and 33% of the Al fraction, respectively). Since the bandgaps of the ABs are much higher (by more than 300 meV in the proposed designs) than the energy of emitted photons in the lasing mode, there will be no absorption of the emission therein and, consequently, it is expected that the presence of ABs (even Al-containing) will not reduce the COMD threshold. Indeed, we did not observe any deterioration of the COMD threshold in the structure with a 7 nm-thick $Al_{0.42}Ga_{0.38}In_{0.2}As$ AB and an $Al_{0.2}Ga_{0.8}As$ waveguide.[8] Nevertheless, we limit here the Al-content in the ABs to suppress the effect of oxidation.

An advantage of the eAB2 design is that it is a common ternary alloy lattice-matched to the substrate. In this design, the useful hole transport is only slightly affected (the h-flux suppression ratio is 8%) while the parasitic e-flux suppression ratio C_e is as high as 76.

As distinct from eAB2, the eAB3 barrier contains a small fraction of antimony ($\approx 4\%$). This enables almost doubling the electron flux suppression ratio ($C_e = 142$) as compared to that in eAB2. The attenuation of the useful hole flux (13%) in this case is due to the fact that a shallow potential well (35 meV) is formed in the valence-band between the heterointerfaces of the waveguide with eAB3—see Fig. 1.

If eAB3 should immediately adjoin the active QW (i.e., there would be no intermediate layer), this shallow well would not affect the hole flux—instead, it would assist in capturing holes into the active region.

It is worth mentioning that one more Al-containing alloy, AlGaPSb, can also be used as a material for the p-side AB. However, the feasible compositions of this alloy contain higher fractions of Al and Sb and provide a lower e-flux suppression ratio C_e compared to the AlGaAsSb quaternary.

The only AB design intended to suppress the parasitic hole flux, hAB, is based on a common ternary compound GaInP containing neither Al nor Sb. It has the highest ratio of parasitic flux suppression (207) among all ABs considered here. This n-side AB has no alternatives as all the other types of alloys offer only poor h-flux attenuation. The combination of this hAB on the n-side and eAB1 on the p-side provides a completely Al-free design of 808 nm AB-lasers.

While the compounds for the eAB1 and eAB3 designs may be considered as somewhat complicated from the viewpoint of epitaxial synthesis, the eAB2 and hAB designs are based on widely exploited ternary alloys (AlGaAs and GaInP, respectively). Hence, the utilization of eAB2 and hAB should not involve any growth complications.

The energy band diagram in Fig. 5 demonstrates the relative positions of the bottoms of the Γ, X, and L valleys in the conduction-band (a) as well as the tops of the heavy-hole, light-hole, and spin-split-hole subbands in the valence-band (b) for the proposed ABs with respect to those in the waveguide material GaInAsP. For the sake of readability, the figure shows only the edges of the X valleys that are transverse to the growth direction. For the compressively strained layers eAB3 and hAB, the bottoms of the longitudinal X valleys are higher than the bottoms of the transverse X valleys by 42 and 32 meV, correspondingly. There is no splitting in the L valleys for the substrate orientation considered here.

It is seen from Fig. 5 that a high energy barrier for Γ electrons can be accompanied by a low barrier for the indirect electron valleys as it takes place, e.g., for X electrons in the structures with eAB2 and eAB3. Moreover, the sign of

FIG. 6. Histogram illustrating the relative contributions of the conduction-band valleys and valence-band subbands to the electron and hole fluxes through the ABs, respectively.

the band edge discontinuity can be different for different valleys. For example, eAB2 forms a 29 meV-high barrier at the X point and a 37 meV-deep well at the L point. Similarly, a potential well is formed for X electrons in the structure with eAB1.

It is also seen from Fig. 5 that the subband discontinuities for heavy and light holes can also be different in the same AB as a result of strain-induced energy shifts, which is the case in eAB3 and hAB.

The stacked-column graph in Fig. 6 shows the relative contributions of the electron valleys and hole subbands to the total fluxes of electrons and holes, respectively, through the ABs. It is seen from the figure that for the p-side ABs eAB1 and eAB3 the X and L valleys dominate in the electron tunnel flux. For example, in the case of the eAB3 layer, the cumulative contribution of the indirect minima is 83%, of which 44% and 39% correspond to the X and L valleys, respectively. It is also seen from the figure that, besides the heavy hole flux, the transport of light holes should be taken into consideration as well—the contribution of this transport to the total hole flux ranges from 13 to 28%. As for the spin-split hole subband, its contribution was found to be negligible due to the large splitting energy in the waveguide material ($\Delta_{so} = 197$ meV) and the presence of energy barriers formed by the ABs for this subband (see Fig. 5).

The significant contribution of the indirect conduction-band minima to the e-flux through the proposed p-side ABs is primarily due to the following: the transport of Γ electrons
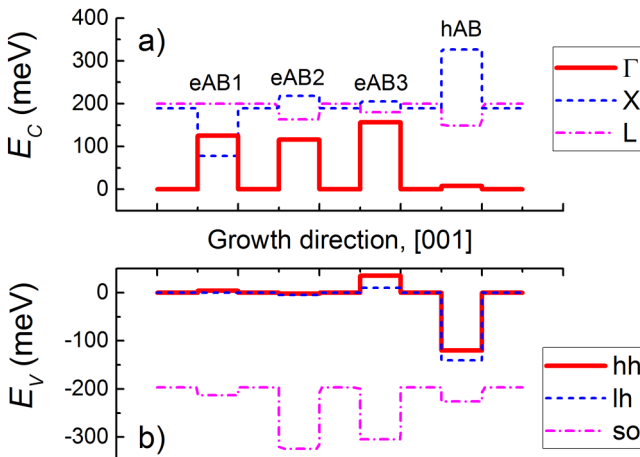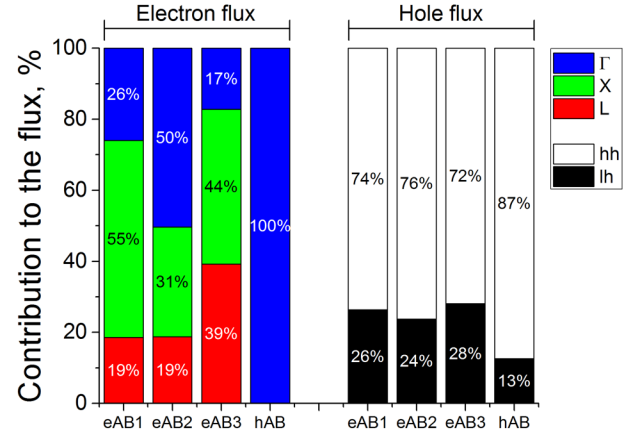

FIG. 5. Conduction-band bottom (a) and valence-band top (b) for different valleys and subbands, respectively. The diagram is presented for three ABs for electrons and one AB for holes incorporated in the waveguide material.

TABLE II. Effective masses (in fractions of the free electron mass) in the conduction-band valleys and valence-band subbands used in our calculations.

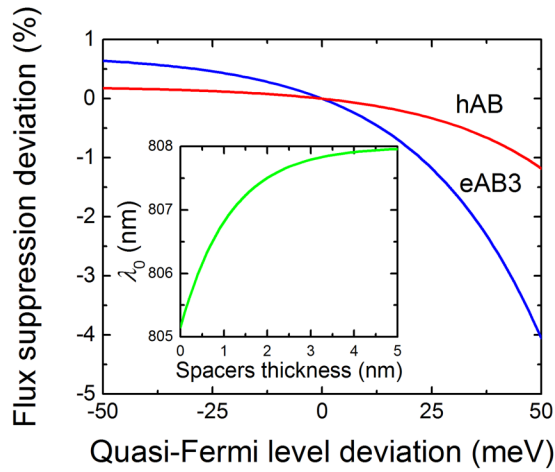| Layer		Waveguide	eAB1	eAB2	eAB3	hAB
Electron effective mass	$m_e^*(\Gamma)$	0.079	0.081	0.087	0.087	0.085
	$m_l^*(X)$	1.552	1.883	1.194	1.201	1.608
	$m_t^*(X)$	0.246	0.257	0.227	0.225	0.299
	$m_{[001]}^*(L)$	0.159	0.198	0.145	0.148	0.199
Hole effective mass	m_{hh}	0.37	0.338	0.389	0.386	0.435
	m_{lh}	0.129	0.155	0.121	0.12	0.157

FIG. 7. Variations in the parasitic electron and hole flux suppression ratios in eAB3 and hAB, respectively, versus the variations in the quasi-Fermi levels around the ground-state energy levels in the QW. Inset: wavelength of the ground-state optical transition in the QW versus the thickness of the intermediate layers (spacers) in a laser with eAB3 and hAB.

is blocked by high energy barriers, while that of X and L electrons is not blocked (see Fig. 5). Another reason for this is the higher effective masses of electrons in these minima compared to that in the Γ valley (Table II). For example, in the case of eAB1, the effective mass in the longitudinal X valley ($m_l^*(X) = 1.883$) is about 23 times as high as that in the Γ valley ($m_e^*(\Gamma) = 0.081$). It follows from Eqs. (1)–(3) that higher effective masses of X- and L-valley electrons make it easier to overcome the energy barriers. For example, our calculations showed that the carrier flux through a 10 nm-wide and a 100 meV-high barrier grows almost linearly with effective mass—it increases by about 18 times as the effective mass increases from 0.1 to 2.

Although we assumed in our calculations that the quasi-Fermi levels are pinned to the corresponding ground-state levels in the active region, they can actually vary with active region temperature and pumping level. However, as our analysis shows, these variations do not affect significantly the parasitic flux suppression ratios by the ABs. Figure 7 shows that C_e and C_h for eAB3 and hAB, respectively, change by less than 4% and 1.2% as the quasi-Fermi levels vary within $\pm 2k_B T$ around the ground-state levels in the QW.

Finally, we discuss the effect of the ABs on the lasing wavelength. The inset in Fig. 7 shows the dependence of the wavelength of the QW ground-state optical transition on the thickness of the intermediate layers (spacers) located between each AB and QW (see Fig. 1). As an example, we consider a laser structure with eAB3 and hAB. There is an insignificant effect of the ABs on the electron and hole energies in the QW, which originates from a slight penetration (about 2 nm) of the electron and hole wave functions into the material adjoining the QW. The inclusion of thin spacers (5 nm-thick in the structure with eAB3 and hAB) almost completely eliminates this effect; as seen from the figure, the lasing wavelength is very close to that in the reference structure (808 nm). It is seen from Fig. 7 that the wavelength slightly

goes down (by 3 nm only) from the designed wavelength of 808 nm as the thickness of the spacers is reduced from 5 nm to zero, i.e., as the spacers are removed.

V. CONCLUSION

It is expected that implementation of auxiliary layers adjoining the active region will significantly enhance the efficiency of lasing and improve the temperature-stability of high-power short-wavelength lasers by suppressing the parasitic recombination in the waveguide layers. Using as an example an 808 nm laser, we showed that the AB-layers concept can be realized in Al-free heterostructures synthesized on GaAs substrates. Moreover, the ABs themselves can be Al-free; for the p- and n-side ABs, we identified $Ga_{0.83}In_{0.17}P_{0.79}Sb_{0.21}$ quaternary and $Ga_{0.47}In_{0.53}P$ ternary alloys with the optimal thickness of 12.6 and 10.5 nm, respectively. These AB layers suppress the parasitic fluxes of electrons and holes by a factor of 53 and 207, correspondingly, while not impeding significantly the useful fluxes—the attenuation of the useful flux of holes is 2% only and that of electrons is 23%. Alternatively, Al-containing alloys (namely, $Al_{0.32}Ga_{0.68}As$ or $Al_{0.33}Ga_{0.67}As_{0.964}Sb_{0.036}$) can be used as the p-side AB for the sake of even better suppression of the parasitic electron flux. The precision of the epitaxial synthesis needed to attain the alloy compositions that satisfy the p-side AB search criteria was estimated to be moderate amounting to $\pm 1\%$. It was found that the effect of ABs on the lasing wavelength is insignificant and can be completely eliminated by either inserting thin (about 5 nm-thick) intermediate layers or slightly tuning the QW width (by less than 10%). We showed that electrons that populate the indirect valleys in the conduction-band can introduce a significant or even dominant contribution to the transport through the ABs. We also showed that light holes should be properly taken into account in addition to heavy holes when considering the hole transport through the ABs.

[1]C. Frevert, P. Crump, F. Bugge, S. Knigge, A. Ginolas, and G. Erbert, "Low-temperature optimized 940 nm diode laser bars with 1.98 kW peak power at 203 K," in CLEO, San Jose, CA, 2015, Paper No. SM3F.8.
[2]P. A. Crump, M. Grimshaw, J. Wang, W. Dong, S. Zhang, S. Das, J. Farmer, M. DeVito, L. S. Meng, and J. K. Brasseur, "85% power conversion efficiency 975-nm broad area diode lasers at – 50°C, 76% at 10°C," in CLEO, Long Beach, CA, 2006, Paper No. JWB24.
[3]P. Crump, W. Dong, M. Grimshaw, J. Wang, S. Patterson, D. Wise, M. DeFranza, S. Elim, S. Zhang, M. Bougher, J. Patterson, S. Das, J. Bell, J. Farmer, M. DeVito, and R. Martinsen, "100-W+ diode laser bars show > 71% power conversion from 790- nm to 1000-nm and have clear route to > 85%," Proc. SPIE **6456**, 64560M (2007).
[4]C. Frevert, P. Crump, F. Bugge, S. Knigge, and G. Erbert, "The impact of low Al-content waveguides on power and efficiency of 9xx nm diode lasers between 200 and 300K," Semicond. Sci. Technol. **31**, 025003 (2016).
[5]P. Crump, H. Wenzel, G. Erbert, and G. Tränkle, "Progress in increasing the maximum achievable output power of broad area diode lasers," Proc. SPIE **8241**, 82410U (2012).

[6]L. V. Asryan, N. V. Kryzhanovskaya, M. V. Maximov, A. Yu. Egorov, and A. E. Zhukov, "Bandedge-engineered quantum well laser," Semicond. Sci. Technol. **26**, 055025 (2011).

[7]A. E. Zhukov, N. V. Kryzhanovskaya, F. I. Zubov, Yu. M. Shernyakov, M. V. Maximov, E. S. Semenova, K. Yvind, and L. V. Asryan, "Improvement of temperature-stability in a quantum well laser with asymmetric barrier layers," Appl. Phys. Lett. **100**, 021107 (2012).

[8]F. I. Zubov, M. V. Maximov, Yu. M. Shernyakov, N. V. Kryzhanovskaya, E. S. Semenova, K. Yvind, L. V. Asryan, and A. E. Zhukov, "Suppression of sublinearity of light–current curve in 850 nm quantum well laser with asymmetric barrier layers," Electron. Lett. **51**, 1106 (2015).

[9]D. Z. Garbuzov, N. Yu. Antonishkis, A. D. Bondarev, A. B. Gulakov, S. N. Zhigulin, N. I. Katsavets, A. V. Kochergin, and E. V. Rafailov, "High-power 0.8 μm InGaAsP-GaAs SCH SQW lasers," IEEE J. Quantum Electron. **27**, 1531 (1991).

[10]L. A. Coldren, S. W. Corzine, and M. L. Mashanovitch, *Diode Lasers and Photonic Integrated Circuits*, 2nd ed. (Wiley, 2012).

[11]A. Al-Muhanna, L. J. Mawst, D. Botez, D. Z. Garbuzov, R. U. Martinelli, and J. C. Connolly, "High-power (>10 W) continuous-wave operation from 100-μm-aperture 0.97-μm-emitting Al-free diode lasers," Appl. Phys. Lett. **73**, 1182 (1998).

[12]D. Botez, "High-power, Al-free coherent and incoherent diode lasers," Proc. SPIE **3628**, 274 (1999).

[13]M. Krakowski, M. Lecomte, N. Michel, M. Calligaro, M. Carbonnelle, M. Tran, M. Lamponi, C. Cayron, V. Ligeret, J. Bébé Manga Lobé, R. Mostallino, N. von Bandel, A. Larrue, Y. Robert, E. Vinet, O. Drisse, M. Garcia, and O. Parillaud, "Review of Al-free active region laser diodes on GaAs for pumping applications," Proc. SPIE **9370**, 93702C (2015).

[14]T. Fukunaga, M. Wada, and T. Hayakawa, "Reliable operation of strain-compensated 1.06 μm InGaAs/InGaAsP/GaAs single quantum well lasers," Appl. Phys. Lett. **69**, 248 (1996).

[15]T. Ohgoh, T. Fukunaga, and T. Hayakawa, "Technologies and applications of Al-free high-power laser diodes," Electr. Eng. Jpn. **158**, 53 (2007).

[16]S. Risemberg, Y. Karni, G. Klumel, M. Levy, Yu. Berk, M. Rech, H. Becht, and B. Frei, "High-power laser diodes at SCD: performance and reliability for defence and space applications," Proc. SPIE **7325**, 73250U (2009).

[17]J. Diaz, H. J. Yi, M. Razeghi, and G. T. Burnham, "Long-term reliability of Al-free InGaAsP/GaAs (λ=808 nm) lasers at high-power high-temperature," Appl. Phys. Lett. **71**, 3042 (1997).

[18]I. Vurgaftman, J. R. Meyer, and L. R. Ram-Mohan, "Band parameters for III–V compound semiconductors and their alloys," J. Appl. Phys. **89**, 5815 (2001).

[19]S. Adachi, *Properties of Semiconductor Alloys: Group-IV, III-V and II-VI Semiconductors* (Wiley, 2009).

[20]Z. G. Zhu, T. Low, M. F. Li, W. J. Fan, P. Bai, D. L. Kwong, and G. Samudra, "Pseudo-potential band structure calculation of InSb ultra-thin films and its application to assess the n-metal-oxide-semiconductor transistor performance," Semicond. Sci. Technol. **23**, 025009 (2008).

[21]C. G. Van de Walle, "Band lineups and deformation potentials in the model-solid theory," Phys. Rev. B **39**, 1871 (1989).

[22]J. E. Matthews and A. E. Blakeslee, "Defects in epitaxial multilayers," J. Crystal Growth **27**, 118 (1974).

[23]R. Tsu and L. Esaki, "Tunneling in a finite superlattice," Appl. Phys. Lett. **22**, 562 (1973).

[24]E. L. Ivchenko and G. E. Pikus, *Superlattices and Other Heterostructures: Symmetry and Optical Phenomena*, 2nd ed. (Springer, 1997).